Citation
Vo, N.H. and Pham, T.M. and Bi, K. and Chen, W. and Hao, H. 2021. Stress Wave Mitigation Properties of Dual-meta Panels against Blast Loads. International Journal of Impact Engineering. 154: ARTN 103877. http://doi.org/10.1016/j.ijimpeng.2021.103877

Stress Wave Mitigation Properties of Dual-meta Panels against Blast Loads

Nhi H. Vo[1], Thong M. Pham[2], Kaiming Bi[3], Wensu Chen[4], and Hong Hao[5]

Abstract

A dual-meta panel functioning as a sacrificial cladding is proposed and its blast mitigation capacity is investigated in this study. The proposed panel possesses the potential to generate bandgaps that target at a specific range of frequencies to stop stress wave propagating through the panel, leading to the favourable stress wave mitigation for structural protection. Aside from the unique stress wave manipulation capability, more energy can be absorbed by a combination of plastic deformation and local resonance. The effectiveness of the proposed panel is validated through numerical simulations. An analytical solution of wave propagation in an ideal meta truss bar is derived to validate the numerical model with good agreement. It is found that the proposed dual-meta panel exhibits an increase in energy absorption, a reduction in transmitted reaction force (up to 30%), and the back plate central displacements (up to 20%) compared to other conventional sandwich panels, e.g. sandwich panel with hollow trusses and solid trusses, in resisting blast loadings. In pursuit of optimizing the performance of the proposed panel, parametric investigations are also conducted to examine the influences of the plate thickness,

[1] PhD Scholar, Center for Infrastructural Monitoring and Protection, School of Civil and Mechanical Engineering, Curtin University, Kent Street, Bentley, WA 6102, Australia. Email: hoangnhi.vo@postgrad.curtin.edu.au

[2] Senior Lecturer, Center for Infrastructural Monitoring and Protection, School of Civil and Mechanical Engineering, Curtin University, Kent Street, Bentley, WA 6102, Australia (Corresponding author). Email: thong.pham@curtin.edu.au

[3] Senior Lecturer, Center for Infrastructural Monitoring and Protection, School of Civil and Mechanical Engineering, Curtin University, Kent Street, Bentley, WA 6102, Australia. Email: Kaiming.bi@curtin.edu.au

[4] Senior Lecturer, Center for Infrastructural Monitoring and Protection, School of Civil and Mechanical Engineering, Curtin University, Kent Street, Bentley, WA 6102, Australia. Email: wensu.chen@curtin.edu.au

[5] John Curtin Distinguished Professor, Center for Infrastructural Monitoring and Protection, School of Civil and Mechanical Engineering, Curtin University, Kent Street, Bentley, WA 6102, Australia (Corresponding author). Email: hong.hao@curtin.edu.au

boundary condition, and the blast load profiles including duration and intensity on the transient response of the proposed dual-meta panel.

Keywords: Metastructure; Dual-meta panel; Sacrificial sandwich panel; Stress wave mitigation; Wave manipulation; Dual-resonator; Blast-resistant structures; Blast loading.

1. Introduction

With the increasing risk of extreme incidents (e.g. explosive and ballistic attacks) worldwide, there are escalating demands for more robust protective structures. Whereas solid monolithic structures [1] and porous materials [2] are currently popular candidates for protective structures, the underlying drivers to refrain from using these types of structures are that they are likely to be cumbersome and bulky. It is, therefore, essential to promote and apply sandwich panels for blast-resistants [3, 4]. The use of sandwich panels attached to main structures as sacrificial cladding were investigated by many researchers, e.g., Hanssen et al. [5]. The role of the panel is to deform in such a way that it absorbs energies from the incident loadings, therefore, minimizing transmitted energy to the protected structure.

Sandwich panels consist of two plates referred as front and back plates separated by a core, have provided promising solutions for energy absorptions from blast loadings. The core comprises materials categorized as cellular foam or lattice type while the plates are often made of thin metals or composite laminates. Generally, sandwich panels can be classified into two categories by the core topology including cellular material cores, e.g. foams [6], kirigami folded [7], honeycombs [8]; and periodic lattice cores, e.g. tetrahedral hollow trusses [9], pyramidal solid trusses [10]. Their means of energy absorption to mitigate dynamic damage rely significantly on plastic deformation mechanisms [7, 11, 12]. For instance, substantial energy can be absorbed by aluminium foams through plastic dissipation [6], thus demonstrating promising potentials against blast loadings. Recently, indebted to the proliferation of the fabrication technology, the core topology developments of sacrificial cladding in blast resistant structures has attracted many researchers. The experimental investigation was carried out to examine the response of the sandwich panel with layered pyramidal truss cores subjected to blast loadings by Wadley et al. [13]. The blast and impact resistance of the sandwich panels was comprehensively presented in a review by Yuen et al. [14]. It was found that the sandwich panels outperform solid plates of the same material and the same mass [15], indicating the significant advantages of the sandwich panels over monolithic plates in blast-resistant functions.

Apart from solely applying the deformation mechanism for blast loading effect mitigation, researchers have approached the problem differently by filtering blast-induced stress wave using the localized resonance mechanism, thus resulting in the loading mitigation. These structures are called metastructures [16], in which the prefix "meta" comes from the Greek preposition and means "beyond", indicating that the characteristics of these structures are beyond what can be seen in nature [17]. The primary concept of these structures is to utilize artificially designed and fabricated structural units to achieve the designed properties and functionalities. In 2016, Li and Tan [18] proposed a meta-lattice truss which is a proportional elastic wave filter based on the unique local resonance of elastic metamaterial to achieve an asymmetric low-frequency bandgap. Subsequently, Li et al. [19] proposed meta-lattice sandwich panels with single-resonators, which show the impact/blast attenuation and higher energy absorption owing to the local resonation of the internal resonator with soft coating. Regarding the dynamic resistance, sandwich structures with lattice cores show better performance compared to the conventional honeycomb sandwich structures [20, 21]. Besides, the application of the metamaterial concept for blast protection has also been found in developing metaconcrete by Jin et al. [22], and Xu et al. [23]. However, despite all these recent works, the relevant research to the application of metamaterials for wave manipulation is still very limited, especially on the comprehensive investigations of the performance of metastructures under blast loadings. Therefore, further studies on this topic are deemed necessary.

This study proposes a new meta sandwich panel with dual-cores as a sacrificial cladding (Fig. 1) by adopting the coupled mechanisms of absorbing strain energy through plastic deformation and local resonance. In this study, the transient responses of the proposed panel against blast loadings are investigated by numerical simulation utilizing LS-DYNA. The bandgap frequency ranges obtained from the numerical simulation are compared with the analytical solution for model validation. For comparison, the responses of the conventional panels – namely solid and hollow truss panel are also simulated to evaluate their blast mitigation capacity compared to the proposed panel. The central displacements of the plates, peak reaction forces, and energy absorption are utilized to assess the performance of panels with different configurations. Parametric studies on the proposed panel are also performed to examine the effects of plate thickness, boundary condition, and blast loading profiles on its transient responses. The results prove that the proposed dual-meta panel possesses superior characteristics that enhance its protective effectiveness against blast loadings compared to its conventional counterparts. Although the physical phenomenon for mitigating effect of the dual-meta panel under blast loading were clearly demonstrated in this study through numerical and analytical analysis, the results also lead to a number of interesting observations, some of which may pave the way for future work through experimental study to comprehensively understand and demonstrate the performance of the dual-meta panel.

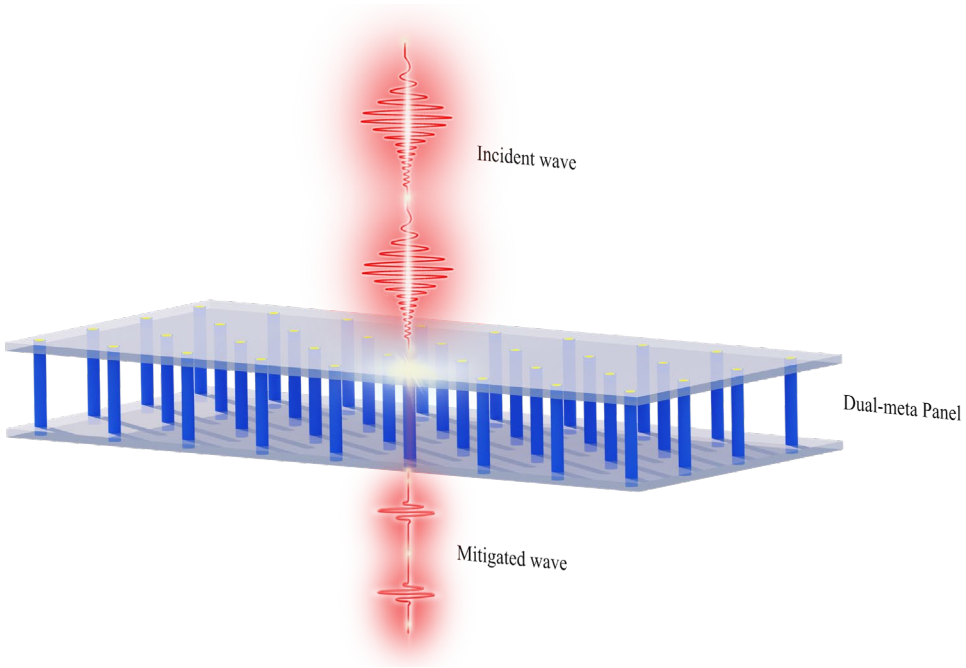

Fig. 1. Schematic diagram of the Dual-meta panel.

2. Design of the Dual-meta panel

Without loss of generality, the proposed dual-meta panel consisting of two thin skins is connected to the meta-lattice trusses as shown in Fig. 2(a). The meta-lattice truss element considered in this study comprises 7 unit cells (Fig. 2(c)). Each unit cell has five parts including the outer tube, two soft coats, and two resonators as shown in Fig. 2(b). The compositions and dimensions of each unit cell are presented in Figs. 2(b) and 2(c), respectively. Aluminium and lead are respectively selected for the tube and the resonators, while the two soft coatings are made from Polyurethane (PU) which can deform elastically to large strain. The two plates are also made of aluminium and connected rigidly to the trusses. As a sacrificial cladding, the perimeter of the back plate is clamped whereas there is no boundary condition imposed on the front plate. All material properties are summarized in Tables 1 and also used in the numerical model in this study.

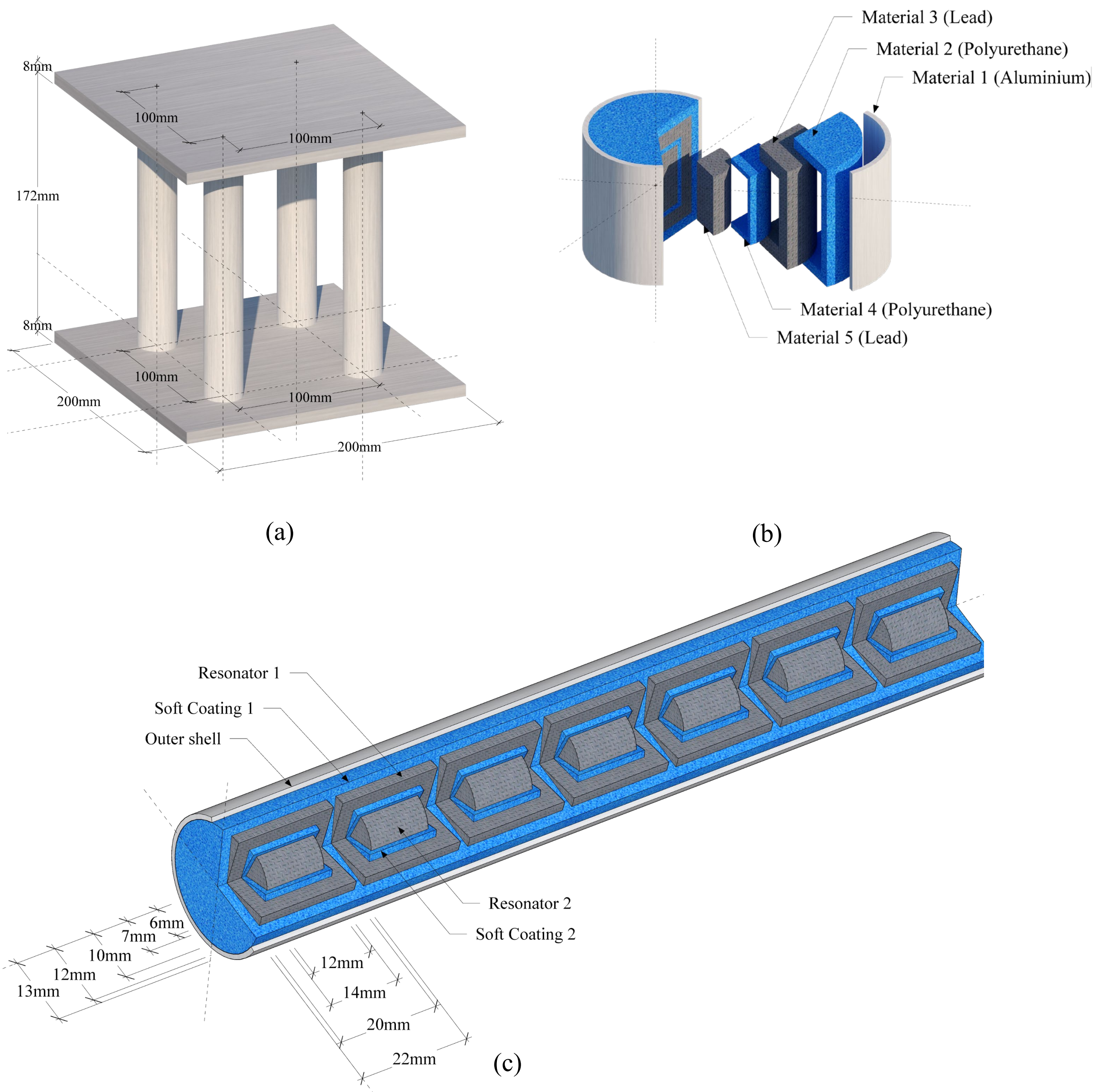

Fig. 2. (a) Schematic view of the dual-meta panel, (b) Unit cell, and c) Meta-lattice truss.

Table 1. Elastic material properties used in the numerical simulation [19], [22]

Properties	Material 1	Materials 2 & 4	Materials 3&5
	Aluminium	Polyurethane	Lead
Density ρ (kg/m^3)	2770	900	11400

Young's modulus E (Pa)	$70\text{x}10^9$	$1.47\text{x}10^8$	$16\text{x}10^9$
Poisson's ratio v	0.33	0.42	0.44

3. Analytical method

A mass-in-mass model can be utilized to analytically describe the diatomic unit cell as depicted in Fig. 3 (a). In the model, the matrix is represented by material 1, i.e., the aluminium truss bar while the two masses of m_1 and m_2 represent the external and internal masses made of material 3 and material 5, respectively. The outer soft coating made of material 2 is modelled by two springs including the outside shear spring k_2 connecting the resonator with the outer truss bar and the axial spring k_1 connecting the adjacent resonators. Similarly, two springs k_3 and k_4 are respectively introduced to describe the axial and shear springs of material 4 connecting the internal mass and external mass.

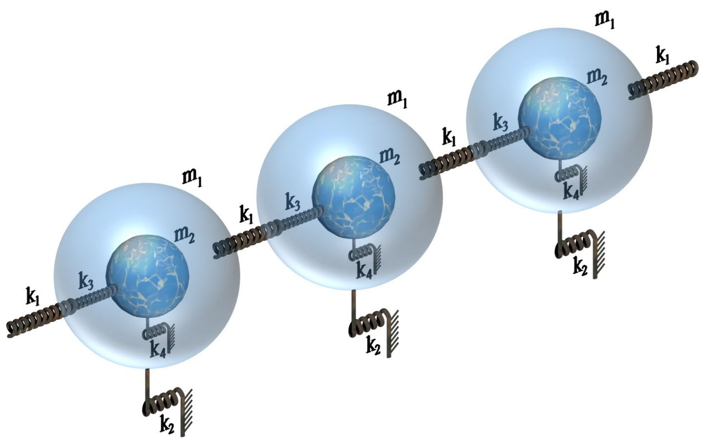

(a)

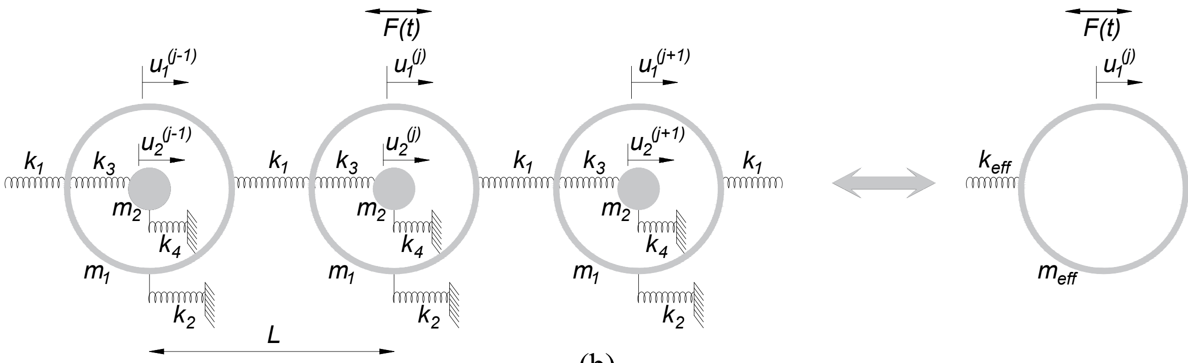

(b)

Fig. 3. (a) Schematic microstructure of infinite dual-core metamaterials, (b) Equivalent effective mass-spring model.

The approximate values of the inner mass and outer mass can be calculated as

$$m_\alpha = \rho_\alpha V_\alpha = \rho_\alpha \pi r_\alpha^2 l_\alpha \qquad \alpha = 1,2 \tag{1}$$

where ρ_α and V_α are the material density and volume of the α^{th} material while the length and radius of the α^{th} unit are denoted by l_α and r_α, respectively.

Besides, the stiffness of equivalent spring can be calculated as follows:

$$k_1 = \frac{E_3 A_1}{l_2}, \qquad k_2 = \frac{G_3 A_2}{l_1}, \qquad G_3 = \frac{E_3}{2(1+\nu_3)} \tag{2}$$

$$k_3 = \frac{E_3 A_3}{l_3}, \qquad k_4 = \frac{G_3 A_4}{l_4}$$

where Young's modulus and shear modulus of the soft material are denoted as E and G, respectively. Due to the shape complexity, the nominal cross-sections of the distinct segments of the soft layer A_i (i=1,2,3,4) presented in the appendix are obtained by FEA. The relevant estimations of the equivalent mass and stiffness are computed as m_1 = 4.71x10^{-2} kg, m_2 = 1.55x10^{-2} kg, k_1 = 57,375 kN/m, k_2 = 35,498 kN/m, k_3 = 40,760 kN/m, and k_4 = 24,802 kN/m.

For an infinite lattice system in which u_1 and u_2 represent the internal and external mass displacements (as shown in Fig. 3(b)). The equations of motion for the j^{th} unit cell can be expressed as:

$$m_1 \frac{d^2 u_1^{(j)}}{dt^2} + k_1\left(2u_1^{(j)} - u_1^{(j+1)} - u_1^{(j-1)}\right) + k_3\left(u_1^{(j)} - u_2^{(j)}\right) + k_2 u_1^{(j)} = 0 \tag{3}$$

$$m_2 \frac{d^2 u_2^{(j)}}{dt^2} + k_3\left(u_2^{(j)} - u_1^{(j)}\right) + k_4 u_2^{(j)} = 0 \tag{4}$$

For harmonic wave solution based on the theory of Floquet-Bloch [24], the displacement of the j^{th} unit cells are given as follows:

$$u^{(j)} = Ue^{i(jqL-\omega t)} \tag{5}$$

where the displacement amplitude and the wavenumber are denoted by U and q, respectively while ω is the angular frequency and L is the length of the unit cell.

The dispersion relation can be obtained by applying the identity $e^{-iqL} + e^{iqL} = 2\cos\left(qL\right)$ and substitute Eq. (5) into Eqs. (3) and (4) as

$$\cos qL = 1 - \frac{m_1\omega^2 - \left(k_2 + k_3\right) + \dfrac{k_3^2}{\left(k_3 + k_4\right) - m_2\omega^2}}{2k_1} \tag{6}$$

The mass-in-mass system can be simplified by a mass-spring system comprising effective mass m_{eff} connecting each other by effective stiffness k_{eff} (Fig. 3(b)). Based on dispersion relation derivation from Eq. (6), the effective mass (m_{eff}) and effective stiffness (k_{eff}) of the equivalent system can be derived as [25]

$$m_{eff} = m_1 - \frac{k_2 + k_3}{\omega^2} + \frac{k_3^2}{\left(k_3 + k_4\right)\omega^2 - m_2\omega^4} \tag{7}$$

$$k_{eff} = k_1 + \frac{1}{4}\left(k_2 + k_3\right) - \frac{1}{4}\left(m_1\omega^2 + \frac{k_3^2}{\left(k_3 + k_4\right) - m_2\omega^2}\right) \tag{8}$$

Applying the transmission equations of the unit cells, the transmission coefficients of the system, T, can be calculated as follows:

$$T = \left|\prod_{j=1}^{N} \frac{u^{(j)}}{u^{(j-1)}}\right| = \left|\prod_{j=1}^{N} T^{(j)}\right| \tag{9}$$

where the wave transmission of the j^{th} and N^{th} unit cells can be expressed as

$$T^{(j)} = \frac{k_1}{k_1\left(2 - T^{(j+1)}\right) - \omega^2 m_{eff}}, \qquad j \in [1, N-1) \tag{10}$$

$$T^{(N)} = \frac{k_1}{k_1 - \omega^2 m_{eff}}, \qquad j = N \tag{11}$$

Based on Eqs. (7), (8), and (9), the analytical dispersion curve of the meta-lattice truss can be calculated and it is depicted in Fig. 4(a), while Figs. 4(b) and 4(c) show the corresponding effective mass and effective stiffness with respect to frequencies, respectively. It is evident that the first and the third bandgaps which are at [0-5] kHz and [13.5-50] kHz are independently formed when the effective mass and the effective stiffness become negative, respectively (see Figs. 4(b) and (c)). Whereas the negativity of both of them collaboratively constitutes the second bandgap which is at [9.3-11.5] kHz (Figs. 4(b) and (c)). It is worth mentioning that the interested frequency range in this study is only up to 50 kHz, covering the frequency band of common blast loads acting on structures [26].

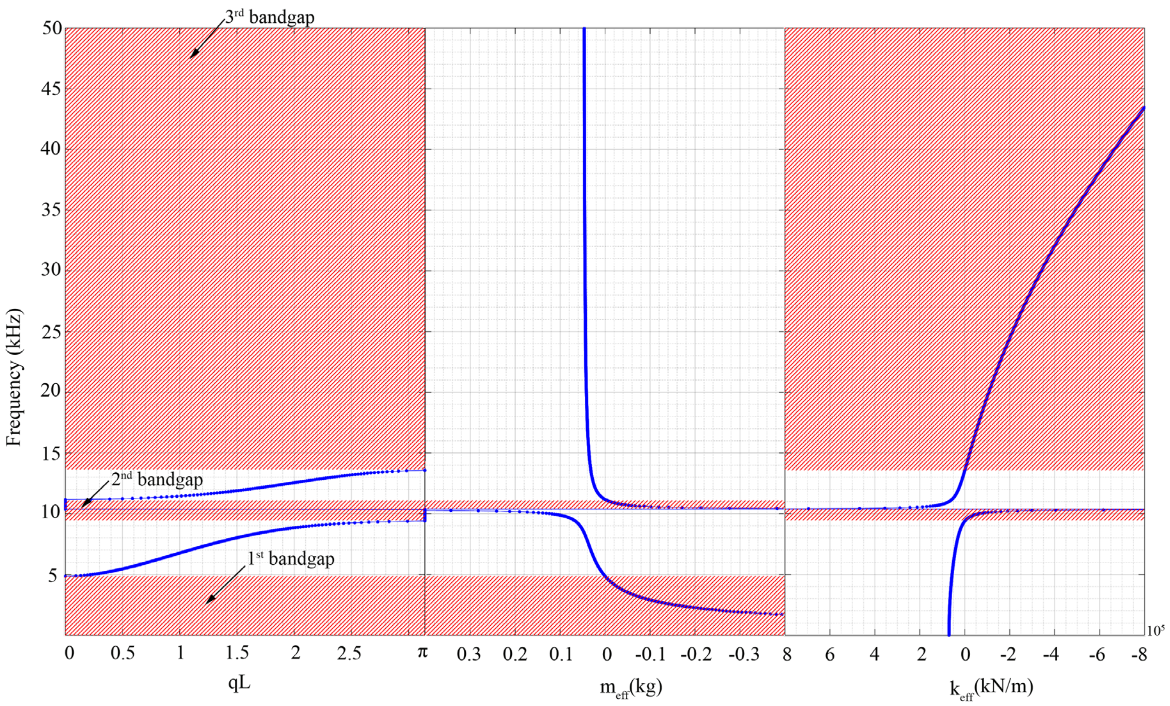

(a) (b) (c)

Fig. 4. Analytical solution of the bandgaps range for meta-lattice truss (a) Dispersion curve, (b) Effective mass, and (c) Effective stiffness.

3. Numerical approach

Owing to the complexity, the infinite unit cells and single harmonic wave assumptions have been applied to analytically solve the Eigen frequency and calculate the bandgaps. Since no study of structural responses and stress wave propagations in the dual-meta panel against the blast loadings has been reported yet, and it is not straightforward to derive such responses analytically, especially when the combined effect of material plastic deformation and meta-lattice truss bandgaps on wave energy dissipation and absorption is considered. The above derivations based on idealized conditions are used in the numerical model to implicitly verify the accuracy of the model. The design of the proposed dual-meta panel and its dimension were presented in Section 2 and shown in Fig. 2.

3.1 Model development

In this study, commercial software LS-DYNA is employed to investigate the characteristics of the dual-meta panel. Constitutive material models, contact definition, initial conditions, element sizes, and blast load modeling are also presented in this section.

3.1.1 *Constitutive material models*

The *MAT_JOHNSON_COOK material (Mat_15) is adopted to capture the behaviour of aluminium while the dynamic behaviour of polyurethane elements is simulated by *MAT_ELASTIC material model due to their distinguished properties [19]. The elastic and plastic material properties are summarized in Tables 1 and 2, respectively. To initialize the thermodynamic state of the material, the Johnson-Cook material model requires an equation of state [27] which is defined by the card *EOS_LINEAR_POLYNOMINAL in which the pressure and initial relative volume are denoted by coefficients C0-C6 and V0, respectively and is presented in Table 3. Furthermore, for simulation of the lead cores, the model *MAT_PLASTIC_KINEMATIC is used and the material properties are given in Table 4 [28]. The Johnson-Cook material model can be expressed as [29]

$$\sigma = \left[A + B\left(\varepsilon^{p}\right)^{n} \right]\left(1 + C\ln \dot{\varepsilon}^{*}\right)\left(1 - T^{*m}\right) \tag{22}$$

where the dynamic yield stress and the equivalent plastic strain are represented by σ and ε^{p}, respectively while $\dot{\varepsilon}^{*} = \dot{\varepsilon} / \dot{\varepsilon}_0$ is the dimensionless plastic strain rate, where $\dot{\varepsilon}_0$ is a reference strain rate which is generally set to 1.0 s^{-1}. Regarding the temperature, $T^{*} = \left(T - T_r\right) / \left(T_m - T_r\right)$ is defined as the homologous temperature, in which T_r and T_m are the material reference and the melting temperature, respectively. In this study, the room temperature (T_r = 20 °C) is applied as the reference temperature [27]. In Eq. (22), there are five material constants including the yield stress determined by the quasi-static compressive strain-stress data represented by A, the influences of strain hardening B and n, the effect of thermal softening m, and the strain rate effect which is represented by C.

Table 2. Johnson-cook material parameters for aluminium [19]

Density (kg/m^3)	Poisson's ratio	Young's Modulus (GPa)	A (Pa)	B (Pa)	C	m	n	T_m	$\dot{\varepsilon}_0$ (1/s)
2770	0.33	70	0.369	0.675	0.007	1.5	0.7	800	1.0

Table 3. Equation of state for aluminium used in the numerical simulation [27]

C_0 (Pa)	C_1 (Pa)	C_2 (Pa)	C_3 (Pa)	C_4	C_5	C_6	E_0 (Pa)	V_0 (m^3/m^3)
0	74.2x10^9	60.5x10^9	36.5x10^9	1.96	0	0	0	1

Table 4. Plastic kinematic material parameters for lead [28]

Density (kg/m^3)	Poisson's ratio	Young's Modulus (GPa)	SIGY (MPa)	ETAN (MPa)	BETA	SRC	SRP	FS	VP (1/s)
11400	0.44	16	20	50	10^9	10^9	1	0	1

3.1.2 *Constraint and initial conditions*

The *BOUNDARY_SPC_SET option in LS-DYNA was adopted to account for the fully clamped boundary along the perimeter of the back plate. The contact between the metals and polyurethane is defined by the keyword *TIED_SURFACE_TO_SURFACE and the keyword *CONTACT_INTERIOR option was utilized for polyurethane to model the slippage and contact failure between materials. Besides, the contact between the outer truss bar and the two plates is defined by the keyword *TIED_NODE_TO_SURFACE to make rigid connections. In this study, all the elements are modeled by the solid hexahedron element (SOLID 164), and the minimum meshing size of 1 mm for all elements is chosen after performing a mesh convergence test, as will be detailed later.

3.1.3 *Blast load modeling*

The keyword *LOAD_BLAST_ENHANCED is widely utilized in LS-DYNA to generate blast load [3, 4] via the CONWEP feature, which takes into consideration the reflection of the blast wave from the surface of the panels. In this study, the blast load on the front plate of the dual-meta panel which considers the enhancement of the reflected waves is defined by this function. The definition of the loading area on the front plate is determined by the keyword *LOAD_BLAST_SEGMENT whereas the function *DATABASE_BINARY_ BLSTFOR is utilized to compute the blast pressure data. The transient blast pressure on the dual-meta panel is determined by the amount of Trinitrotoluene (TNT), the stand-off distance, and the angle of incidence. The blast pressure is computed by the following equation [30]

$$P(t) = P_r \cos^2\theta + P_i\left(1 + \cos^2\theta - 2\cos\theta\right) \tag{23}$$

where θ is the angle of incidence. The incident pressure and the reflected one are denoted by P_{i} and P_{r}, respectively. These peak pressures are calculated by the scaled distance, $Z = R / W^{1/3}$, in which R and W are the stand-off distance and the amount of TNT, respectively. In this study, 0.15 kg TNT is detonated at a distance of 0.35 m above the front plate of the dual-meta panel, which corresponds to the scaled distance of 0.65 m/kg$^{1/3}$. The reflected pressure time history at the center point of the front plate and the corresponding FFT spectrum are illustrated in Fig. 5. As shown, the peak reflected pressure is approximately 13.5 MPa and the dominant blast loading energy distributes in the frequency band up to 50 kHz.

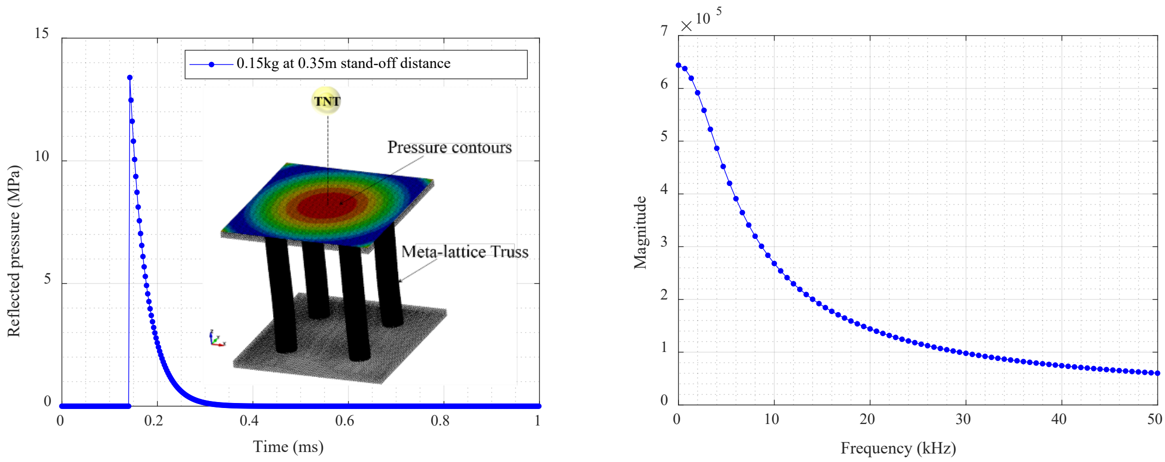

(a) (b)

Fig. 5. Peak reflected pressure profile (a) Time history, and (b) FFT spectrum.

3.2 Mesh convergence test

A convergence test is necessary to be carried out to determine the size of elements in finite element modeling for computational accuracy and efficiency. To obtain the optimal solution, different mesh sizes comprise 3 mm, 2 mm, 1 mm, 0.5 mm, and 0.25 mm representing coarse, medium, and fine meshes are considered in the convergence test. The calculated displacements at the central point of the back plate of the dual-meta panel corresponding to the various mesh sizes are shown in Fig. 6. It can be seen from the figure that the displacement becomes converged when the mesh size is 1 mm. Further reducing the mesh size does not considerably affect the predicted displacement but increases significantly the computational cost. The mesh size of 1 mm is, therefore, utilized in the subsequent investigations.

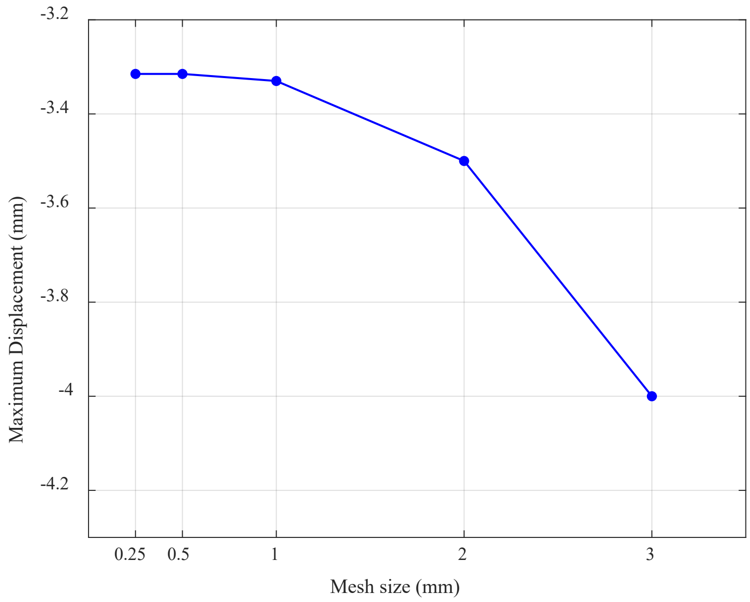

Fig. 6. Effect of mesh sensitivity on the maximum displacement of the back plate.

3.3 Model validation

To validate the numerical simulation, the transmission coefficient of a single truss bar calculated by the numerical simulation is compared with that obtained by the above analytical derivation. The transmission coefficient is the ratio between the output and the input signals of the structure. For the numerical simulation, the input signal defined by a sweep frequency ranging from 0 – 50 kHz is applied at one end of the meta-lattice truss, and the displacement response at the other end is calculated to derive the transmission coefficient. The numerical transmission coefficient of the meta-lattice truss is shown in Fig. 7 along with the analytical result. The numerical simulation shows that the meta-lattice truss possesses three bandgaps at the frequency ranges of [0-5] kHz for the 1st bandgap, [8.1-11.8] kHz for the 2nd bandgap, and [13.3-50] kHz for the 3rd bandgap, while the corresponding ranges from the analytical solution are [0-5] kHz, [9.3-11.5] kHz, and [13.5-50] kHz as presented above. These results indicate that the numerical results agree closely with the theoretical transmission coefficient, implying the validity of the model. The slight variations in the bandgaps between the analytical and the oscillations of the numerical results are because the meta-lattice truss is assumed continuous with an infinite number of unit cells connected by springs in the analytical derivation, while the numerical meta-lattice truss has a finite length with 7 unit cells only, and each component is modelled with its respective elastic material property and density instead of the lumped mass connected with idealized springs.

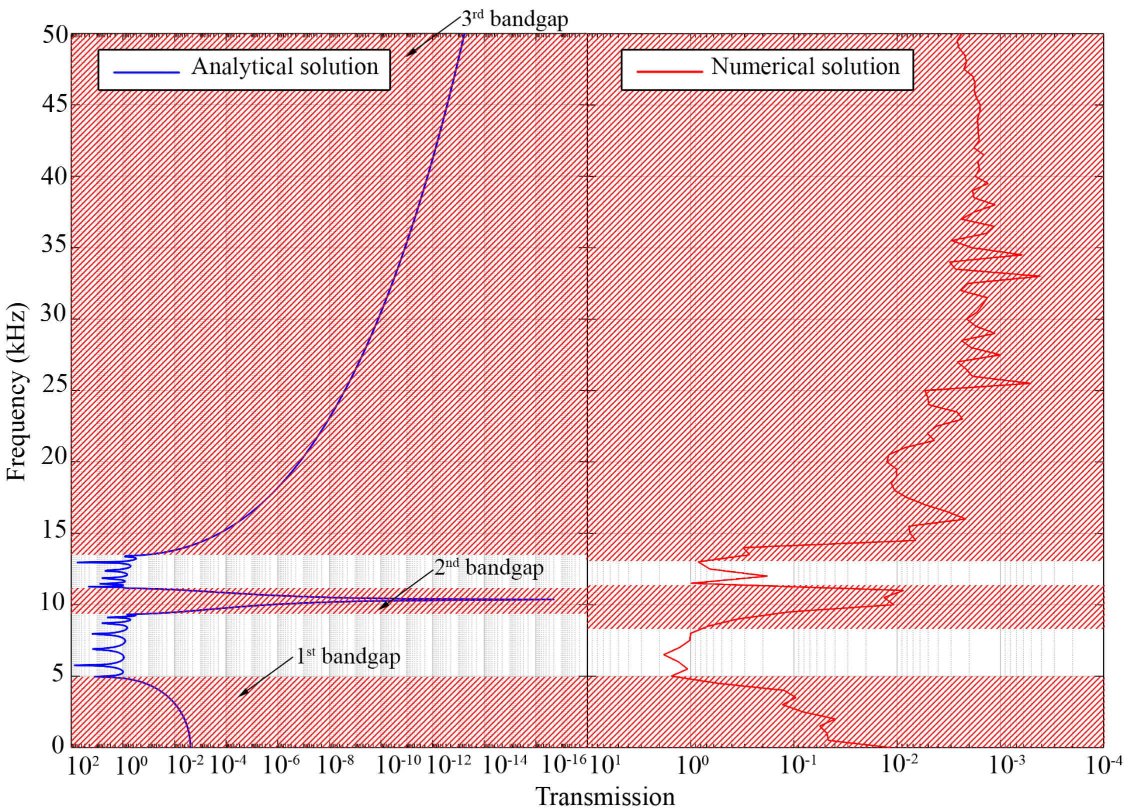

Fig. 7. Transmittance profiles of meta-lattice truss under sweep frequency input: analytical analysis vs numerical simulation.

To further testify the frequency suppression capacity of the meta-lattice truss, an excitation is generated by a prescribed displacement time history with multi-frequency components [31] as

$$u(t) = 10^{-4}\left[\sin(2\pi f_1 t) + \sin(2\pi f_2 t) + \sin(2\pi f_3 t)\right] H(t) \tag{12}$$

where the unit-step function *H(t)* is defined as

$$H(t) = \begin{cases} 1, & t \geq 0 \\ 0, & t < 0 \end{cases} \tag{13}$$

and f_1=2 kHz, f_2=7 kHz, and f_3=10 kHz. This excitation is applied at one end of the meta-lattice truss to calculate the response at its other end. Fig. 8 shows the displacement time history at the two ends of the meta-lattice truss (i.e. the input and the output, respectively). It is worth mentioning that f_1 and f_3 are intentionally designed to fall within the first and the second bandgap, respectively, while f_2 is within its passband range. Theoretically, only the signal with f_2 can pass while other signals will be stopped by the metacores. The FFT spectrum of the input and output signal are shown in Fig. 9. As shown, only one input signal with the frequency of 7 kHz can pass through the meta-lattice truss while the other two signals at frequencies 2 kHz and 10 kHz are suppressed by the meta-lattice truss.

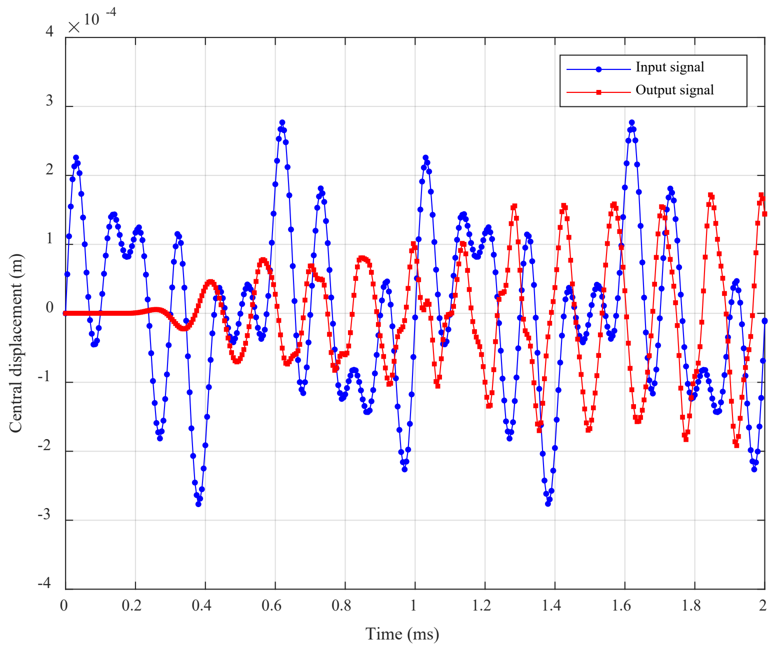

Fig. 8. Input and Output displacement time histories at the center points of two ends of the meta-lattice truss.

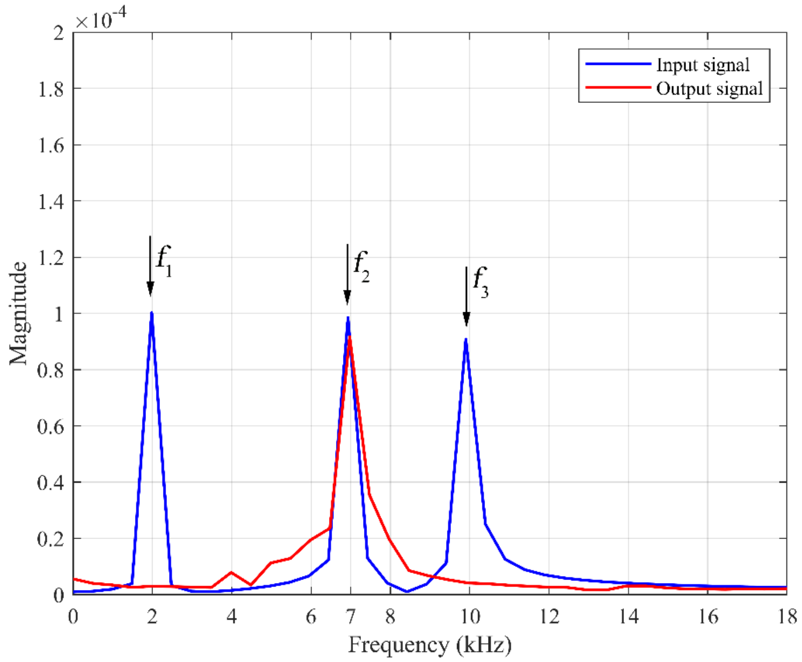

Fig. 9. The Fourier spectrum (FFT) of the input and output displacements at the center points of two ends of the meta-lattice truss.

3.4 Results and discussions

To further demonstrate the extraordinary characteristics of the dual-meta panel in resisting blast load, responses of the proposed dual-meta panel consisting of four meta-lattice truss bars (shown in Fig. 2) subjected to the blast loads defined in Fig. 5 are calculated. For comparison, two conventional sandwich panels with solid trusses and hollow trusses as shown in Fig. 10(a) and 10(b), respectively, are also modelled. As shown in Fig. 10, the two conventional sandwich panels have the same geometries and dimensions as the proposed dual-meta panel. The only difference among the three panels is the truss bars connecting the two plates. The diameter of the solid truss bar is the same as the meta-lattice truss bar, and the hollow truss bar is the same as the outer hollow tube of the meta-lattice truss bar. It should be noted that the total weight of these three structures are not the same. To make the total weight of the three structures the same, the size of the solid and hollow truss bars need be adjusted. Since the primary objective of this study is to investigate the performance of the meta-lattice truss bar in mitigating the blast loading effect, the size of the truss bars are kept the same instead of making the weight the same in the analysis. It is because to keep the mass constant in the study, the thickness and/or diameter of the hollow truss and the solid truss need be adjusted, which affects the stiffness of the core and hence the deformation and energy absorption of the structure. Specifically, the wall of the hollow truss will be thicker or its diameter larger compared to the current referenced hollow truss because the mass has to be increased to match the mass of the soft coats and the lead cores. Similarly, the diameter of the solid truss has to be increased because the density of the lead core is higher than the aluminium tube. This would increase the stiffness of the core and decrease the deformation and the energy absorption of these panels. This phenomenon can be seen from the results that the hollow truss panel outperforms the solid truss panel as a sacrificial cladding for blast resistance due to its higher energy absorption capacity. However, it should be noted that increasing the mass enhances the inertial resistance of the structure, hence the structural capacity to resist the blast load. Although the primary design targets of a sacrificial panel are energy absorption and load transferred to the protected structure, instead of the loading resistance capacity of the sacrificial structure itself, it would be interesting to also compare the performance of the proposed dual-meta panel with reference panels having the same mass. Nonetheless the scenario of the three panels having the same mass is not considered in this investigation, but it is believed that increasing the mass of the traditional panels with hollow truss and solid truss bars would reduce their energy absorption capacity and increase the loading amplitude acting on the protected structures because of the increased stiffness of the core. Responses of the three panels subjected to the same blast loads, including displacement response at the center point of the back plate, total energy absorption, and the boundary reaction force are compared to examine the effectiveness of the proposed panel on structure protections.

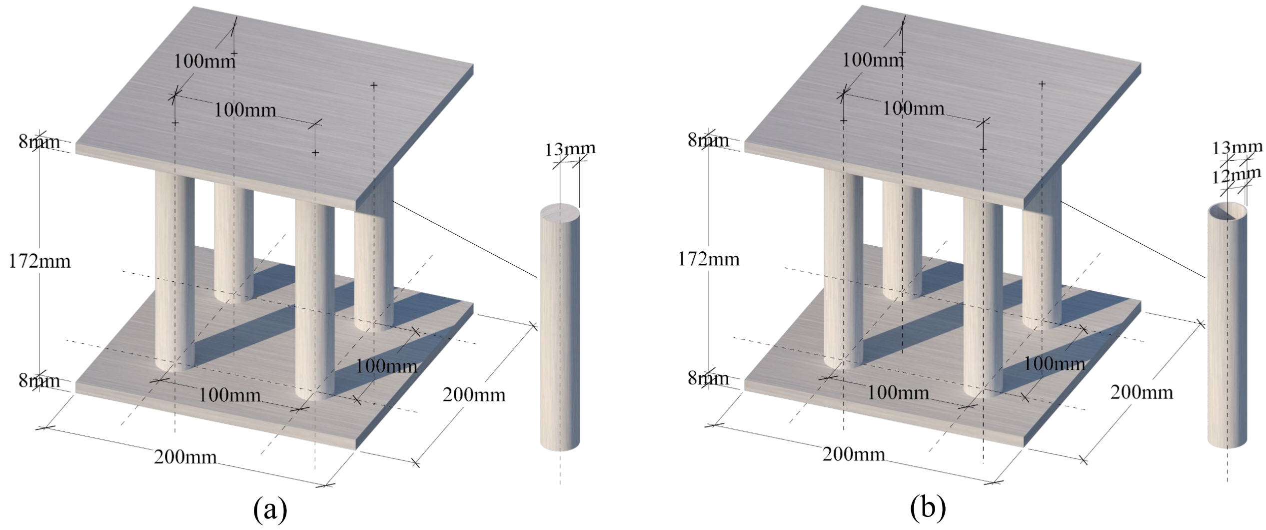

Fig. 10. Schematic view of the sandwich panels with (a) Solid trusses and (b) Hollow trusses.

Fig. 11 compares the displacement time histories at the center point of the back plate of the three panels. It is seen that the panel with solid trusses has a higher maximum displacement (i.e. 4 mm), followed by the panel with the hollow trusses (i.e. 3.81 mm). The corresponding maximum displacement of the dual-meta panel is 3.36 mm, i.e., 13.5%, and 20.0% lower than that of the hollow truss panel and solid truss panel, respectively. It is also noted that there is a substantial reduction in the second negative peak displacement in comparison between the dual-meta panel with the panels with solid truss (i.e. 40.9%) and hollow truss (i.e. 52.0%). These can be attributed to the fact that the effect of metacores results in lower impulse transfer to the lower plate of the panel. Placing the metacores inside the truss bars of the panel results in a considerable reduction of the maximum peak central displacement of the back plate compared to the conventional panel, indicating the dual-meta panel has better protective performances.

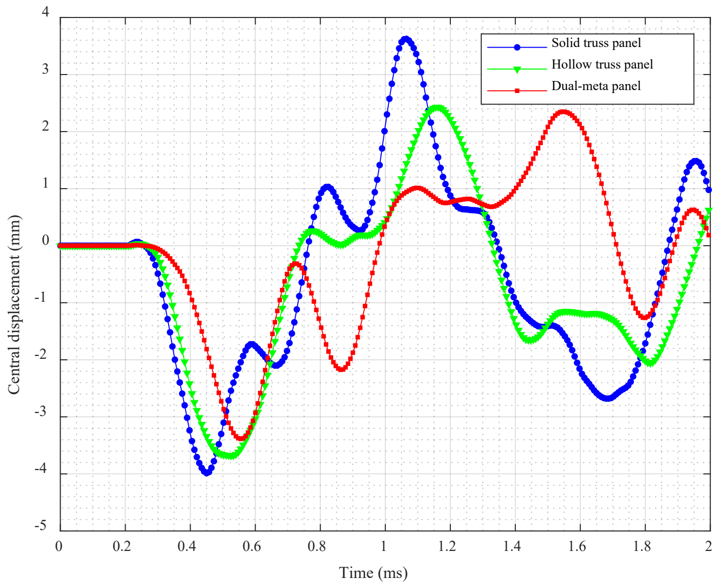

Fig. 11. Time histories of central point displacement of the back plate of the three panels.

To gain a comprehensive insight into blast response mitigation, investigations on the energy absorption of the dual-meta panel are carried out. The total energy (E_t), the kinetic energy (E_k), and the internal energy (E_i) absorbed by each component of the dual-meta panel subjected to blast loading are shown in Figs. 12(a), (b), (c), respectively. It should be noted that, since the energy fluctuates in the time histories, the estimated energy in this study is its mean values. It is observed that the amount of energy absorbed by the metacores and the soft coating is generally higher than that of the outer hollow truss bars. The energy absorption by the hollow truss bars is mainly associated with its plastic deformation, while the energy absorption by the metacores and soft coatings is primarily caused by local vibrations of the cores. These results indicate the damage to the truss bars by the blast load is reduced because of the local vibrations of the metacores. As shown, the outer hollow tubes of the metatruss bars experience plastic deformation which also consumes energy imparted to the panel (Fig. 12 (c)), whereas the relative movement of the metacores contributes mainly to kinetic energy (Fig. 12 (b)) and partly to the internal energy due to the deformation of the coatings. These results indicate the dual-meta panel possesses the high energy absorption capability through the local vibration of the metacores, which not only protects the back plate of the sandwich structure but also reduces the damage to the outer hollow tube of the metatruss bars. Fig. 12 (d) shows the movements of each component in the panel including the two plates, the outer tube, the soft coatings, and the cores. It is worth noting that there are out-of-phase motions between the metacores and the outer tube due to the existence of the soft coatings, which effectively mitigate the blast loading effect on the back plate.

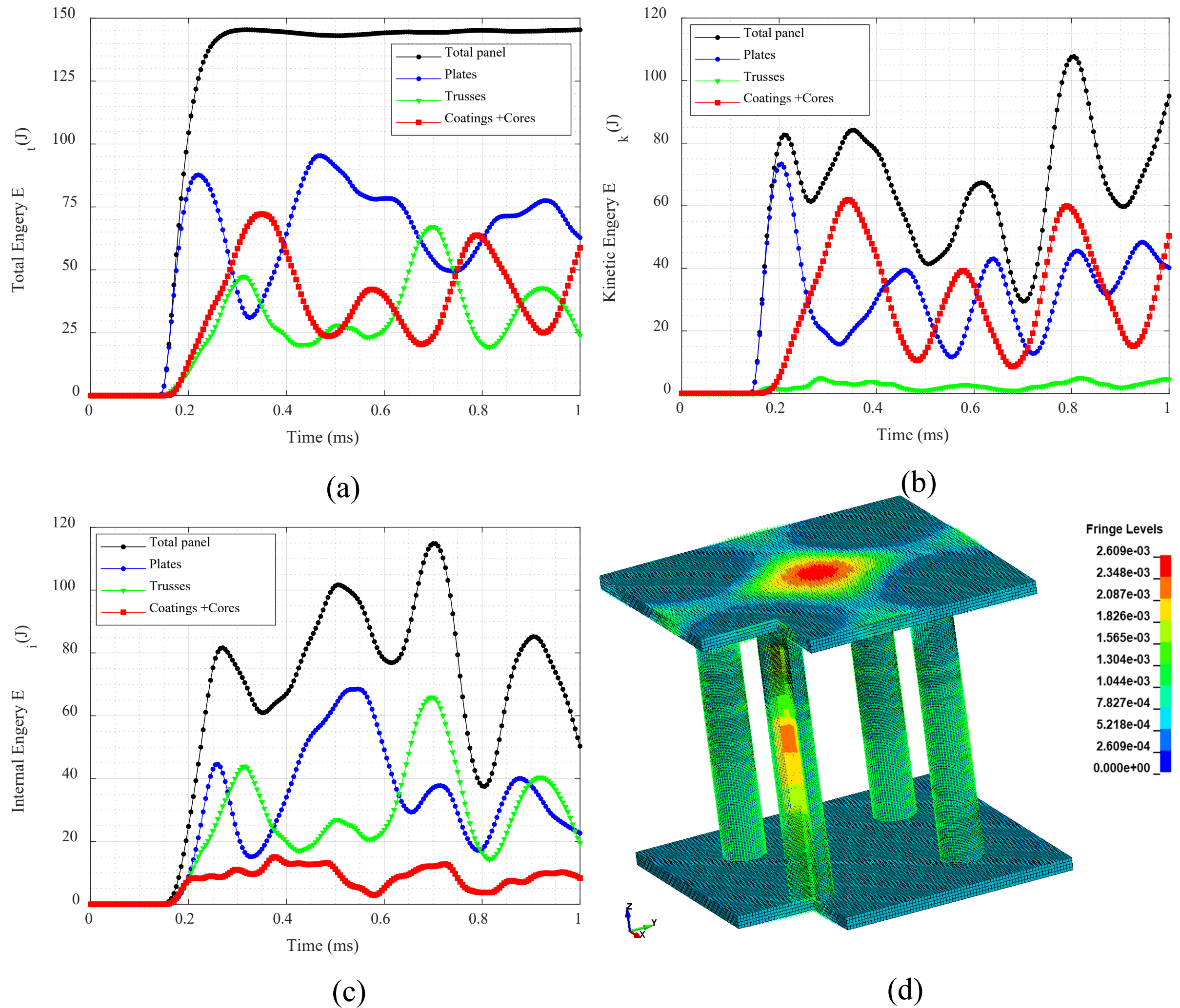

Fig. 12. Energy time histories of each component of the dual-meta panel (a) Total energy, (b) Kinetic energy, (c) Internal energy, and (d) Displacement contour of each component of the dual-meta panel.

For comparison, the energy absorptions of the two reference panels are also calculated. The total energy absorption of the whole panel and each component of the three panels are shown in Fig. 13. The dual-meta panel shows the highest total energy absorption. Among the three panels, the panel with solid truss bars absorbs the least amount of energy, and in which the most energy absorption is due to the plastic deformation of the plates, indicating the least protective effectiveness. The panel with hollow truss bars absorbs energy through plastic deformation of the plates and the truss bars. The energy absorbed by the hollow truss bars is the largest compared to the solid and meta-lattice truss bars, implying the largest plastic deformation of the hollow truss bars. The energies absorbed by the plates and the truss bars of the dual-meta panel are the smallest among the three panels although the dual-meta panel absorbs more energy than the two reference panels, indicating the smallest plastic deformation and hence the mitigation of damages to plates and outer hollow truss bars. These results further demonstrate the good performance of the proposed dual-meta panel.

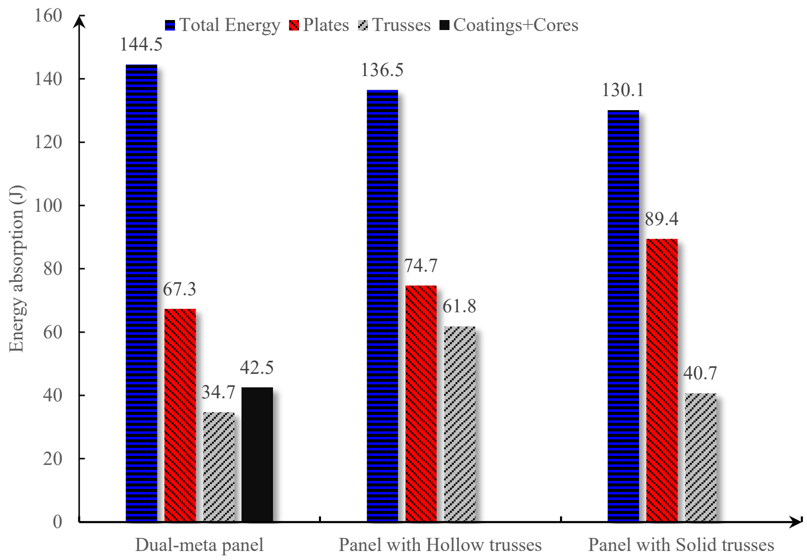

Fig. 13. Energy absorption of the three panels.

The reaction force in Z-direction (F_z) along the boundary of the back panel is also a key factor for the assessment of the protective effectiveness of the sacrificial panels. To evaluate this factor, the reaction force time histories of the three panels are shown in Fig. 14. It is worth mentioning that the investigated reaction force is the sum of the reaction forces distributed around the boundary. As observed, the dual-meta panel is effective in reducing the reaction force of the sandwich panel. The maximum reaction force of the dual-meta panel is 18.2% and 30.1% less compared to that of the hollow truss and solid truss panels, respectively. The reaction force of the dual-meta panel almost stabilizes (25 kN) after the first positive peak at 2 ms while the second positive peaks of the reaction force of the other two panels are still large (90~115 kN which is comparable to the first peak). The second positive peak of the reaction force of the dual-meta panel reduces by 72% and 78% as compared to that of the panel with the hollow truss and solid truss core, respectively. This is because the metacores filter out the stress from the blast loading due to the relative movement of the metacore and the soft coating, thus less stress from the blast load is transferred to the back plate and then the supports. The reaction force at the supports, therefore, reduces which in turn relieves the demand on support designs of the sandwich panel and loading on the protected structure.

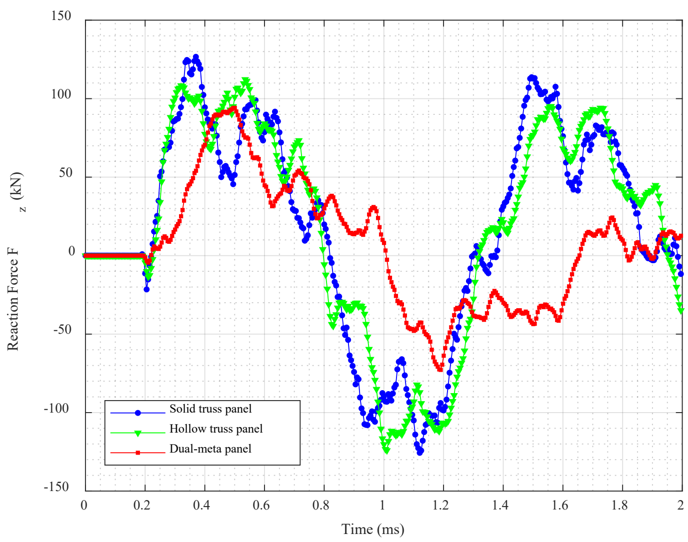

Fig. 14. Comparison of the reaction force time histories of the three panels under blast loading.

The effective performance of the dual-meta panel is further evaluated by analyzing the von Mises stress distribution of the back plate. Fig. 15 shows the stress contours at the back plates of the dual-meta panel, solid truss panel, and hollow truss panel, respectively. As shown in the figure, the back plate exhibits the stress concentration at the connections between the truss bars and the back plate since the blast loading generates the stress wave propagating through the truss bars. The results clearly show that the von Mises stresses in the back plate of the dual-meta panel is the smallest among the three panels, while that of the solid truss panel is the largest, indicating again the effectiveness of the stress wave mitigation capability of the dual-meta panel.

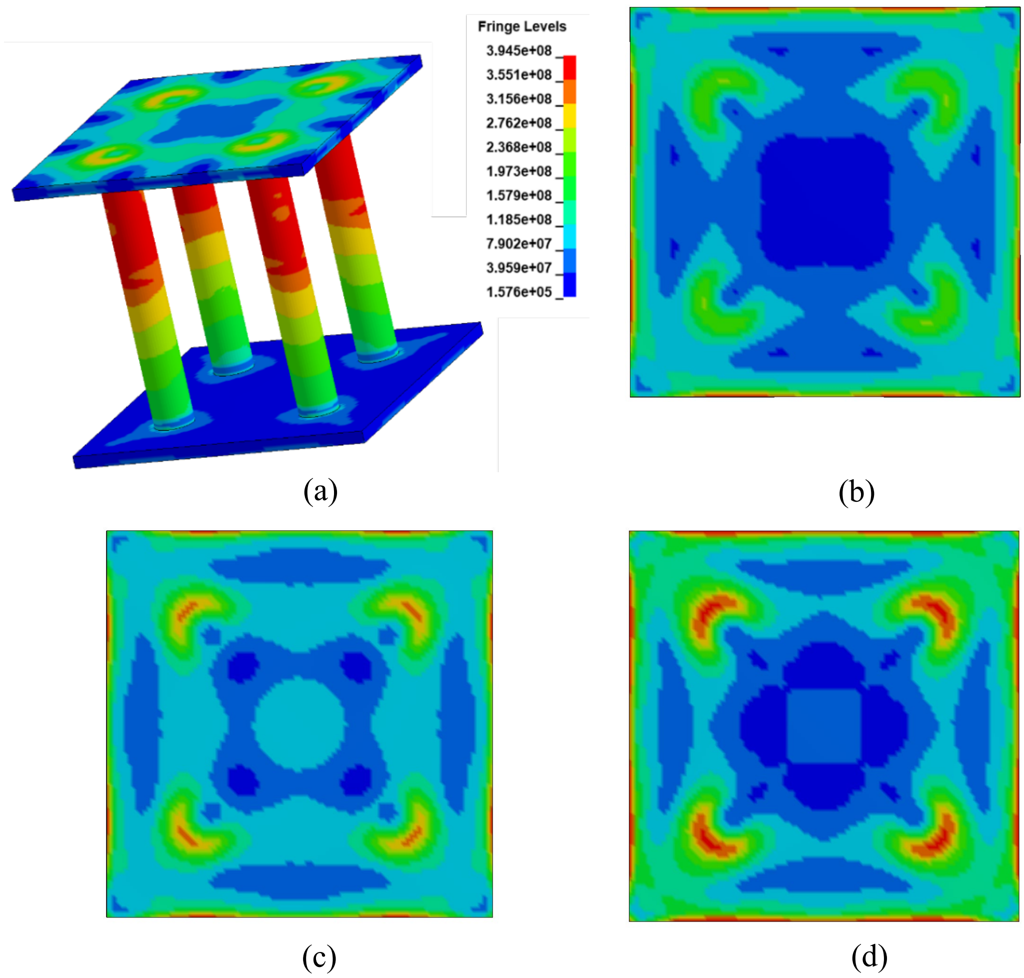

Fig. 15. (a) Stress contours of 3D dual-meta panel and stress contours at the back plate of (b) Dual-meta panel, (c) Hollow truss panel, and (d) Solid truss panel.

To further compare the blast resistance of the panels with the same mass, two other conventional panels with hollow truss bars and solid truss bars are also considered. The masses of these panels are kept the same as that of the dual-meta panel and thus the diameter of the truss bars of these three panels are different. Geometries of these panels and the blast loading are kept the same as described in Section 3.4 except for the diameter of the solid truss bar and the thickness of the hollow truss bar, which are adjusted to have the same mass as the meta-truss bar. The solid truss bar has the radius of 25.5 mm and the hollow truss bar has the outer and inner radii of 28 mm and 12 mm, respectively. The results show that the energy absorption of these panels (i.e. 74.1 J and 69.5 J for panels with hollow trusses and solid trusses, respectively) are significantly smaller than that of the dual-meta panel (144.5 J). Therefore, it demonstrates again that the dual-meta panel outperforms the same mass conventional panels.

In summary, the proposed dual-meta panel reduces the maximum displacement of the back plate (up to 20.0% for the first peak and 52.0% for the second peak) and the reaction forces (up to 30.0% for the first peak and 78.0% for the second peak), and absorbs more energy compared to the conventional panel with solid and hollow truss bars. The local vibration of the metacores also reduces the stress and plastic deformation of the truss bars and the back plates of the sandwich panel, therefore mitigates the damages to these components of the panel. These results demonstrate the better performance of the dual-meta panel as a sacrificial cladding to resist blast loading than the conventional sandwich panels with solid and hollow truss bars.

3.5 Parametric investigations

In this section, the influences of critical parameters such as the thickness of the plate, boundary condition, blast load duration and intensity on the performance of the dual-meta panel are numerically investigated. This section is carried out to gain further insights into the performance of the dual-meta panel subjected to confined blast loading as a sacrificial cladding.

3.5.1 *Effect of the thicknesses of the plates*

Herein, the transient response of the dual-meta panel is examined with varying front plate thickness while keeping the back plate thickness unchanged and vice versa. Three thicknesses, i.e. 4 mm, 6 mm, 12 mm, are taken into consideration. Therefore, six panels with different combinations of thicknesses of front plate and back plate are considered in this section including 4 mm (F) + 8 mm (B), 6 mm (F) + 8 mm (B), 12 mm (F) + 8 mm (B), 8 mm (F) + 4 mm (B), 8 mm (F) + 6 mm (B), and 8 mm (F) + 12 mm (B). Figs. 16 (a) and (b) depict the central deflection of the back and front plates with varying plate thicknesses. It should be noted that the above plate configurations are determined to obtain a more comprehensive and valid comparison on protective effectiveness, i.e, the panels experience different levels of deformation without failure. This predetermined condition also assumes these panels after deformation would not touch the main structure and only transfer the load to the main structure through their supports. As expected, the deflections of both the front and back plates decrease with the increase of their thicknesses. Drastic reduction in displacements by increasing the plate thickness demonstrates its significance in suppressing the blast loading of the dual-meta panel. It is noted that in most cases, the displacement at the central point of the front plate is smaller than that of the back plate due to their boundary conditions. The four edges of the back plate are restrained in all directions while the edges of the front plate are free. The displacement of the overhanging portion of the front plate would counteract its central point displacement resulting in a reduction in the displacement amplitude. As shown in Figs. 16 (c) and (d), with an increase in the thickness of the front plate from 4 mm to 12 mm, there is an increase in the reaction force and a substantial reduction of the total energy absorption. This phenomenon happens mainly because the less deflection of the plate means less energy absorption through its plastic deformation. In brief, the reaction force is highly sensitive to the front plate thickness and it is not beneficial to use a thick front plate in the design of sacrificial panels.

Regarding the influence of the thickness of the back plate, when changing its thickness, the first peak displacement of the front plate is the same but the second peak displacement and the subsequent displacement responses vary. This is attributed to the stress waves generated by the blast load transfer from the front plate to the back plate. Regardless of the thickness (thus stiffness) of the back plate, the front plate will be the first component to resist the blast load, its first peak displacement, therefore, is not sensitive to the thickness of the back plate. However, its second peak displacement is affected by the stiffness of the back plate owing to the reflected stress and deformation of the back plate. It is observed that the second peak displacement occurs when the panel rebounds from its first peak and it moves back in the opposite direction. Meanwhile, the reaction force and the total energy absorption are not sensitive to the thickness of the back plate. In brief, the displacement of the plate is highly sensitive to the stiffness of the plate, due to the correlation between the stiffness and the displacement. While the thickness of the back plate only affects its own displacement, reducing the front plate thickness results in smaller reaction forces and absorbing more energy. From Fig. 16, it can be seen that the two good combinations are 4 mm (F) + 8 mm (B) and 8 mm (F) + 4 mm (B) since they absorb more energy compared to its total amount of materials. However, the combination of 8 mm (F) + 4 mm (B) exhibits a much higher reaction force than that of 4 mm (F) + 8 mm (B). Hence, the optimal design of the dual-meta panel as a sacrificial cladding should have a fairly thin front plate and a thick back plate to fully manifest its protective performance such as high energy absorption and less deflection of the back plate. It is noted that the effect of the plate's thicknesses on the blast mitigation of the dual-meta panel is similar to that of other blast-resistant sandwich panels [3].

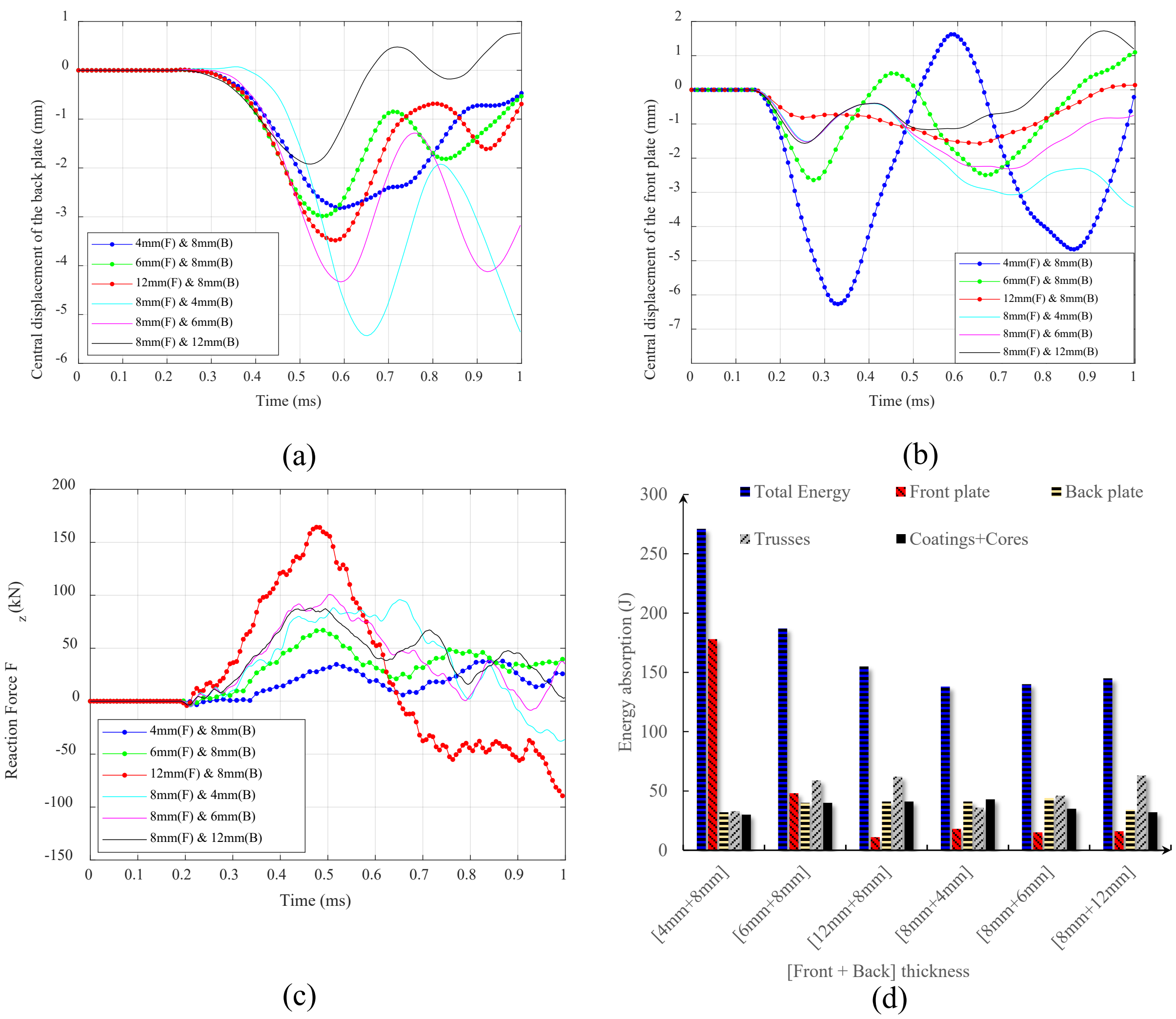

Fig. 16. Effects of the plate thickness on dual-meta panel dynamic response time histories (a) Central displacement of the back plate, (b) Central displacement of the front plate, (c) Reaction force, and (d) Total energy absorption of various components.

3.5.2 *Effect of boundary conditions*

The boundary condition determination relies on how sacrificial claddings can be utilized in structural protection [32]. There are various ways that the protective panel can be attached to the main structure, namely, clamped or pinned at the edges allowing some clear space between the panel and the protected structure, or directly fixed against the system without a gap. In this study, these attachment methods are considered with three boundary conditions including all perimeter is clamped, simply pinned, and all the surface of the back plate is fixed, i.e., directly attaching the panel on the protected structure. The transient responses of the dual-meta panel with these selected boundary conditions subjected to the same blast loading (defined in Fig. 5) are compared in Fig. 17 and Table 5. As shown in Fig. 17, the central displacement of the back plate of the panel with pinned boundary is 13.1% larger than that with clamped boundary condition. Meanwhile, the plates and the metacores of the pinned panel witness a decrease in energy absorption compared to the clamped panel by 16.7 % and 20.7 %, respectively. However, the energy absorbed by the truss bars of the clamped panel is lower than that of the pinned panel. Therefore, the total energy absorption of the panel with the pinned and fixed boundary conditions differs by only 1 %. As for the case with the fixed back surface, the energy absorbed by the trusses is higher compared to that of the other two boundary conditions because the constraints of the lower plate result in more deformation of the trusses leading to more energy absorption. The total energy absorption of the fully fixed panel is comparable to that of the panel with clamped boundary, implying the amount of energy absorbed by the back plate deformation is compensated by the larger plastic deformation of the outer tube of the truss bars. The reaction force in the Z-direction of the panel with the fully fixed back surface is two times higher than those of the panel with other boundary conditions, therefore, it is not recommended to apply the fixed back surface in practice. Moreover, the reaction force with the clamped condition is slightly higher than that of the pinned condition. In summary, the displacement and the energy absorption by various parts of the panel are significantly affected by the boundary conditions while it exerts less influence on the total energy absorption of the panel. This conclusion is in good agreement with other blast-resistant sandwich panels such as aluminium foam-cored sandwich panels [33]. For practical applications, the dual-meta panel will perform better as a sacrificial cladding if there is a gap between it and the protected structure, with less blast force transferred to the protected structure, but concentrated at the supports. Directly attaching the panel on the protected structure also leads to larger plastic deformations of the outer tube of the truss bars, making the metacores less effective in absorbing blast energy.

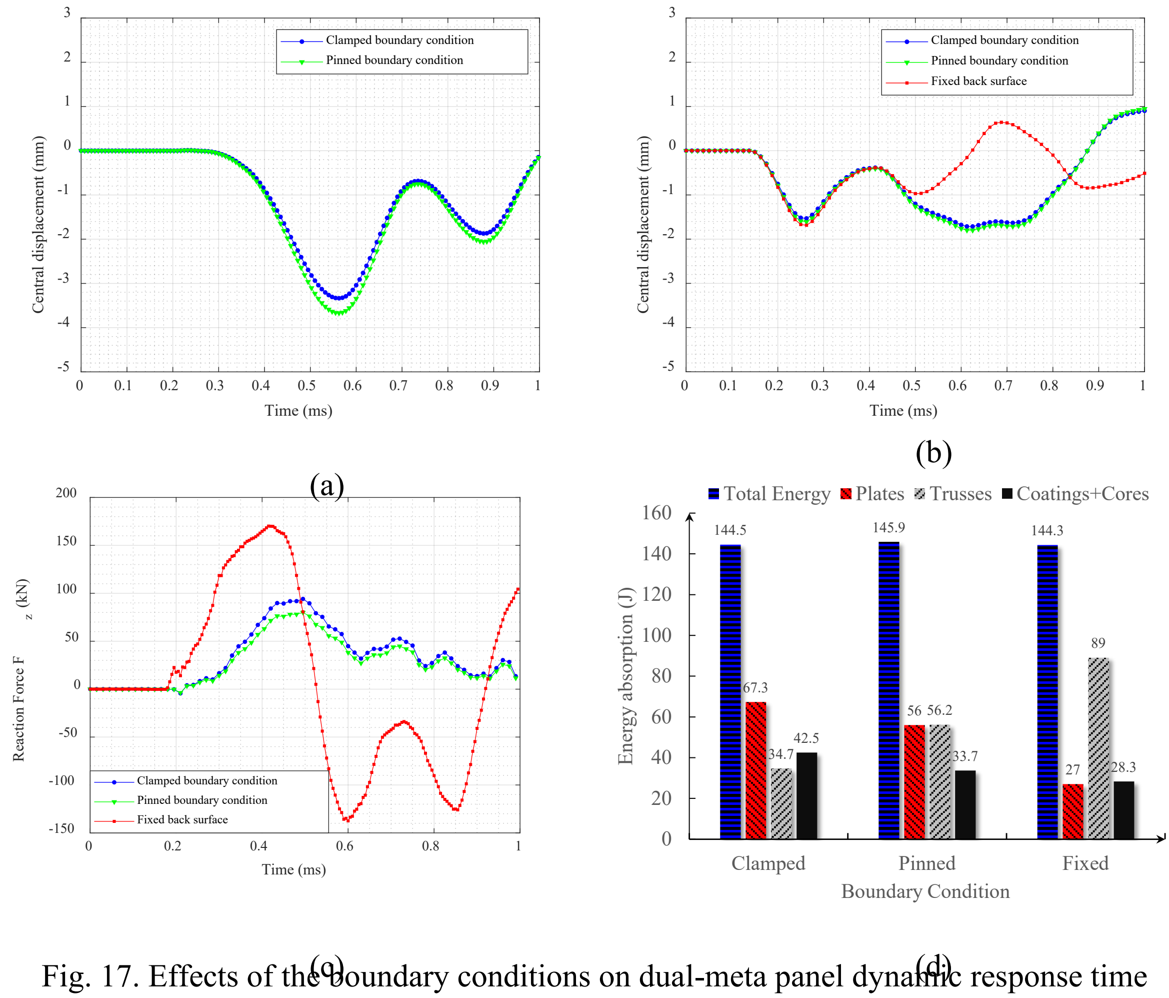

Fig. 17. Effects of the boundary conditions on dual-meta panel dynamic response time histories (a) Central displacement of the back plate, (b) Central displacement of the front plate, (c) Reaction force, and (d) Total energy absorption of various components.

Table 5. Effects of boundary conditions on displacements, reaction force, and energy absorptions.

Boundary condition	Displacement (mm)				Reaction force (kN)		Energy absorption (J)			
	Front plate	Reduction	Back plate	Reduction	F_z	Reduction	Plate	Trusses	Coatings + Cores	Total
Clamped	1.55	N/A	3.33	N/A	91.5	N/A	67.3	34.7	42.5	144.5
Pinned	1.57	-1%	3.81	-13.1%	82.7	10.6%	56.0	56.2	33.7	145.9
Fixed	1.74	-12%	N/A	N/A	170.1	-85.9%	27.0	89.0	28.3	144.3

3.5.3 *Effects of blast loading duration and intensity*

To comprehend the influence of different levels of blast loading duration on a given dual-meta panel, four blast loading profiles (shown in Fig. 18) with different duration but the same amplitude are considered. The blast loading profile is defined by using the modified Friedlander's equation [34]:

$$F = F_{\max}\left(1 - \frac{t - t_0}{t_d}\right) e^{-\frac{t - t_0}{t_d}},\ t_0 \le t < t_0 + t_d \tag{14}$$

$$F = 0,\ t < t_0 \text{ or } t \ge t_0 + t_d$$

where $F_{\max}$ is the amplitude while the time constants t_o and t_d are the blast initial time and blast duration, respectively. In this study, the negative phase in the blast loading profile is neglected in the analysis [35]. For different loading regimes, durations t_d of 0.1 ms, 0.2 ms, 0.3 ms, and 0.4 ms are chosen in the analyses. It should be noted that the blast loading duration is purposedly chosen relatively short to generate a wider loading frequency band for evaluating the performance of the dual-meta panel in mitigating the blast loading effect. In an explosion case, such short loading duration could be associated to contact and very close-in explosions. With the amplitude F_{max} of 13.5 MPa, the corresponding impulses are 530.8 Ns, 1027.2 Ns, 1523.8 Ns, and 2020.4 Ns, respectively with the four different duration. It is obvious when varying the duration of the blast loading, the dominant frequency band of the blast loading would change accordingly. The corresponding blast loading energy in the three bandgaps of the current meta-lattice trusses can be calculated by the area (A_{bandgap}) enclosed by the FFT spectrum of the blast loading in each bandgap as illustrated in Fig. 18(b). The portion of the blast loading energy corresponding to each bandgap is calculated by dividing the energy in each bandgap by the total blast loading energy (A_{total}), and are given in Table 6. As shown, more proportion of energy from blast load with longer duration falls into the bandgaps of the dual-meta panel, i.e, 77.0%, 81.0%, 82.4%, and 83.4%, respectively for the four considered loading cases, implying the dual-meta panel is more effective in mitigating the blast loading effect from load with the longest considered duration in this study.

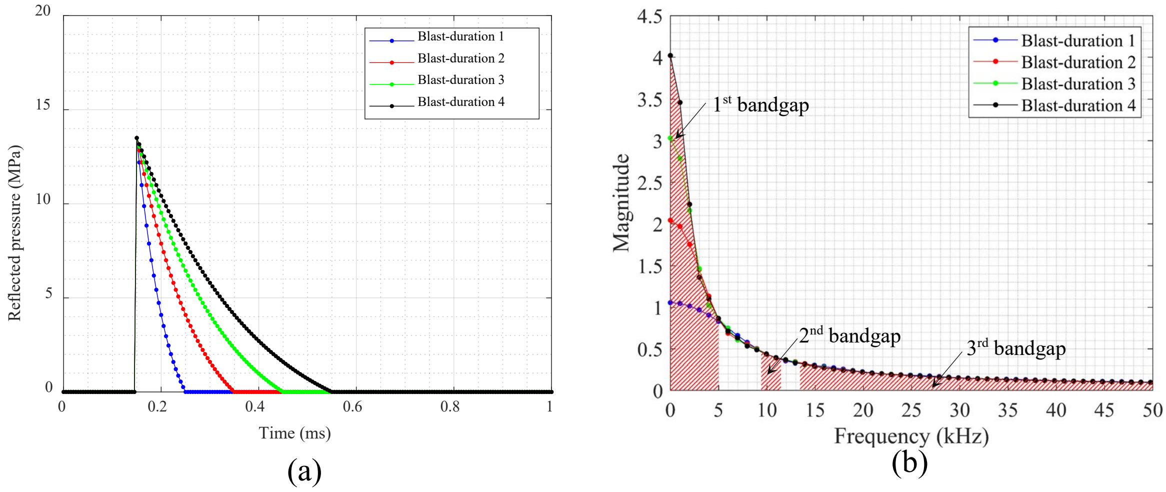

Fig. 18. Blast loading profiles with different duration, (a) Time histories, and (b) FFT spectra.

Table 7 gives the dynamic response of the dual-meta panel subjected to the assumed blast loads with different duration uniformly applied to the front plate of the panel. The results indicate that the dynamic responses of the dual-meta panel rely heavily on the blast loading impulse. The plate deflections, the reaction forces, and the energy absorption of the panel increase with the loading impulse. It is obvious that the effectiveness of the dual-meta panel in blast load mitigation depends on the frequency band of the blast loading, therefore, aside from the total energy absorption increases from loading case 1 to case 4 due to the increased blast loading energy imparted to the structure, the largest percentage of energy absorption by the coatings and the cores of the meta-lattice trusses corresponds to the loading case 4, which is 392/1188=32.9% as shown in Table 7, followed by 31.9%, 29.6%, and 28.7%, respectively for the loading cases 3 to 1. This is because the proportion of the blast energy of the loading cases considered in the analyses reduces from case 4 to case 1, implying the meta-lattice truss can stop more blast loading energy transmission as shown in Fig. 18(b) when more proportion of the blast loading energy falls into the bandgaps. It should be noted that the percentage of energy absorption of the coatings and the cores in the dual-meta panel calculated from Table 7 is smaller than the corresponding values in Table 6. It is because the energy absorption of the dual-meta panel is constituted by four components, i.e., the plates, the truss bars, the coatings, and the cores. Only the metacores including the coatings and the cores have the bandgap-related mitigating capability, while the plates and trusses absorb energy through plastic deformation.

Table 6. Proportion of blast loading energy with different duration falling in the bandgaps of the single meta-lattice truss.

Blast loadings	**1st bandgap**		**2nd bandgap**		**3rd bandgap**		**Total**
	$\frac{A_{\text{bandgap}}}{A_{\text{total}}}$	%	$\frac{A_{\text{bandgap}}}{A_{\text{total}}}$	%	$\frac{A_{\text{bandgap}}}{A_{\text{total}}}$	%	%
Blast-duration 1	$\frac{4875}{15340}$	31.7%	$\frac{927}{15340}$	6.0%	$\frac{6039}{15340}$	39.3%	77.0%
Blast-duration 2	$\frac{7746}{17976}$	43.1%	$\frac{929}{17976}$	5.1%	$\frac{5903}{17976}$	32.8%	81.0%
Blast-duration 3	$\frac{9364}{19580}$	47.8%	$\frac{929}{19580}$	4.7%	$\frac{5855}{19580}$	29.9%	82.4%
Blast-duration 4	$\frac{10570}{20740}$	50.9%	$\frac{926}{20740}$	4.4%	$\frac{5835}{20740}$	28.1%	83.4%

Table 7. Effect of blast loading duration on displacements, reaction force, and energy absorption.

Blast loadings	**Displacement (mm)**		**Reaction force (kN)**	**Energy absorption (J)**			
	Front plate	**Back plate**	**F_z**	**Plates**	**Trusses**	**Coatings + Cores**	**Total**
Blast-duration 1	1.7	4.1	120	95	46	57	198
Blast-duration 2	2.6	7.3	190	253	136	164	553
Blast-duration 3	3.1	9.7	230	392	212	283	887
Blast-duration 4	3.5	11.2	270	528	268	392	1188

To evaluate the effectiveness of the dual-meta panel subjected to blast load with different peaks but the same impulse, the responses of the dual-meta panel subjected to blast load with the impulse of 530.8 Ns but varying the peak pressure and duration. The blast loading duration of

0.1 ms, 0.2 ms, 0.3 ms, and 0.4 ms with the corresponding peak pressure of 13.5 MPa, 6.75 MPa, 4.5 MPa, 3.375 MPa, respectively are considered. Figure 19 shows the blast loading time histories and the corresponding FFT spectra of these blast loading profiles. The portions of the blast loading energy in each bandgap of the meta-lattice trusses are given in Table 8. The corresponding percentages of the blast loading energy falling into the bandgaps of the panel are 77.0%, 80.9%, 82.2%, and 83.4%, respectively for Blast loading case 1-4 as shown in Table 8.

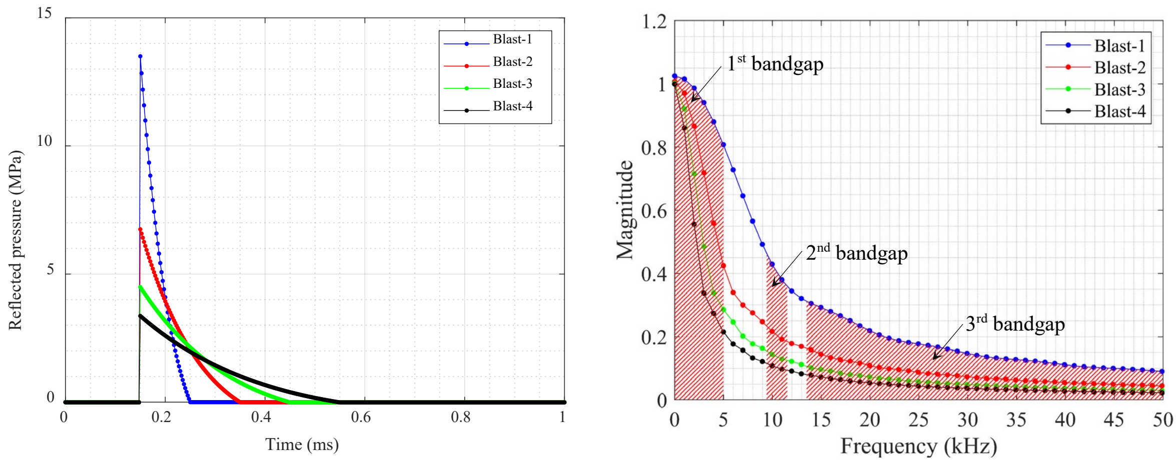

(a) (b)

Fig. 19. Blast loading profiles with different duration and intensities (a) Time histories, and (b) FFT spectra.

As shown in Table 9, the plate displacements and energy absorption of the dual-meta panel decrease with the reduction of the peak blast load given the same impulse. Also, the highest peak reaction force corresponds to the loading Blast-1, which is reasonable since it is associated with the highest peak blast load. As given in Table 9, although the total energy absorption increases from the loading Blast-4 to Blast-1 due to the increase of the peak blast load, the largest percentage of energy absorption by the coatings and the cores corresponds to Blast-4, which is 26/76=34.2%, followed by 32.5%, 30.1%, and 28.7%, for Blast-3 to Blast-1, respectively. It is again attributed to the proportion of the blast loading energy falling into the bandgaps given in Table 8. These results demonstrate that the transient responses of the dual-meta panel correlate with the peak blast load and its capacity to absorb energy in the bandgap ranges. Therefore, the proposed dual-meta panel can be designed to maximize its blast load mitigation efficiency for an expected blasting scenario.

Table 8. Proportion of blast loading energy with different duration and intensities falling in the bandgaps of the single meta-lattice truss.

Blast loadings	**1st bandgap**		**2nd bandgap**		**3rd bandgap**		**Total**
	$\frac{A_{\text{bandgap}}}{A_{\text{total}}}$	%	$\frac{A_{\text{bandgap}}}{A_{\text{total}}}$	%	$\frac{A_{\text{bandgap}}}{A_{\text{total}}}$	%	%
Blast-1	$\frac{4875}{15340}$	31.7%	$\frac{927}{15340}$	6.0%	$\frac{6039}{15340}$	39.3%	77.0%
Blast-2	$\frac{3877}{9010}$	43.1%	$\frac{465}{9010}$	5.1%	$\frac{2958}{9010}$	32.8%	81.0%
Blast-3	$\frac{3125}{6543}$	47.8%	$\frac{310}{6543}$	4.7%	$\frac{1956}{6543}$	29.9%	82.4%
Blast-4	$\frac{2646}{5198}$	50.9%	$\frac{232}{5198}$	4.4%	$\frac{1462}{5198}$	28.1%	83.4%

Table 9. Effects of blast loading duration and intensities on displacements, reaction force, and energy absorption.

Blast loadings	**Displacement (mm)**		**Reaction force (kN)**	**Energy absorption (J)**			
	Front plate	**Back plate**	**F_z**	**Plates**	**Trusses**	**Coatings + Cores**	**Total**
Blast- 1	1.7	4.1	120	95.0	46.0	57.0	198
Blast- 2	1.3	3.6	109	63.2	34.0	41.8	139
Blast- 3	0.9	3.2	97	42.5	25.0	32.5	100
Blast- 4	0.8	2.8	87	30.8	19.2	26.0	76

4. Conclusions

The capability of the proposed dual-meta panel to attenuate blast loading effect is examined in this study. Theoretical derivations and numerical simulations are carried out to investigate the mechanism and responses of the dual-meta panel against blast load. The proposed dual-meta panel is aimed to increase the blast resistance capacity, whilst maintaining a low base reaction force. The key points found from the study can be enumerated as follows:

1. Compared to the conventional sandwich panel with solid and hollow truss core, the panel with dual-meta truss core has smaller central peak deflections of the back plate (up to 20% for the first peak and 52% for the second peak), smaller reaction force (up to 30% for the first peak and 78% for the second peak), and absorbs more blast loading energy, demonstrating that the dual-meta panel has the potential for significantly enhancing the dynamic performance of the cladding and outperforms its conventional counterparts.

2. The performance of the dual-meta panel on blast loading mitigation depends on the structural configurations. A relatively weak front plate and stronger back plate, and separating the sacrificial dual-meta panel from the protected structure with a small gap lead to better protective effectiveness of the panel in terms of energy absorption and the level of load transmitted to the protected structure.

3. The performance of the dual-meta panel also depends on the blast loading profile and energy distribution. The dual-meta panel with bandgaps consistent with the primary blast loading energy distribution in the frequency domain is more effective in mitigating the blast loading effect.

The study proves that the dual-meta panel holds great potential for extensive applications in various engineering fields requiring blast load mitigation.

Acknowledgments

The authors would like to acknowledge the financial support from the Australian Research Council via Laureate Fellowships FL180100196 and the Research Training Program Scholarship (RTP) from Curtin University.

References

[1] D.K. Sahoo, A. Guha, A. Tewari, R.K. Singh, Performance of Monolithic Plate and Layered Plates Under Blast Load, Procedia Engineering, 173 (2017) 1909-1917.

[2] A.N. Rotariu, C. Dima, E. Trană, C. Enache, F. Timplaru, L.C. Matache, Uninstrumented Measurement Method for Granular Porous Media Blast Mitigation Assessment, Experimental Techniques, 40 (2016) 993-1003.
[3] W. Chen, H. Hao, Numerical study of blast-resistant sandwich panels with rotational friction dampers, Int. J. Struct. Stab. Dyn., 13 (2013).
[4] W. Chen, H. Hao, Numerical Simulations of Stiffened Multi-arch Double-layered Panels Subjected to Blast Loading, Int J Prot Struct, 4 (2013) 163-188.
[5] A.G. Hanssen, L. Enstock, M. Langseth, Close-range blast loading of aluminium foam panels, Int J Impact Eng, 27 (2002) 593-618.
[6] Z. Li, W. Chen, H. Hao, Dynamic crushing and energy absorption of foam filled multi-layer folded structures: Experimental and numerical study, Int J Impact Eng, 133 (2019) 103341.
[7] Z. Li, W. Chen, H. Hao, Blast mitigation performance of cladding using square dome-shape kirigami folded structure as core, Int J Mech Sci, 145 (2018) 83-95.
[8] J. Liu, Y. Li, X. Shi, W. Wang, Dynamic Response of Bird Strike on Aluminum Honeycomb-Based Sandwich Panels, Journal of Aerospace Engineering, 27 (2014) 520-528.
[9] E.C. Clough, J. Ensberg, Z.C. Eckel, C.J. Ro, T.A. Schaedler, Mechanical performance of hollow tetrahedral truss cores, International Journal of Solids and Structures, 91 (2016) 115-126.
[10] M. Li, L. Wu, L. Ma, B. Wang, Z. Guan, Structural design of pyramidal truss core sandwich beams loaded in 3-point bending, Journal of Mechanics of Materials and Structures, 6 (2011) 1255-1266.
[11] Z. Li, W. Chen, H. Hao, Blast resistant performance of cladding with folded open-top truncated pyramid structures as core, 2018.
[12] Z. Li, W. Chen, H. Hao, Numerical study of blast mitigation performance of folded structure with foam infill, Structures, 20 (2019) 581-593.
[13] H. Wadley, K. Dharmasena, Y. Chen, P. Dudt, D. Knight, R. Charette, K. Kiddy, Compressive response of multilayered pyramidal lattices during underwater shock loading, Int J Impact Eng, 35 (2008) 1102-1114.
[14] S.C.K. Yuen, G.N. Nurick, M.D. Theobald, G.S. Langdon, Sandwich Panels Subjected to Blast Loading, in: A. Shukla, G. Ravichandran, Y.D.S. Rajapakse (Eds.) Dynamic Failure of Materials and Structures, Springer US, Boston, MA, 2010, pp. 297-325.
[15] Z. Xue, J.W. Hutchinson, Preliminary assessment of sandwich plates subject to blast loads, Int J Mech Sci, 45 (2003) 687-705.
[16] A. Silva, F. Monticone, G. Castaldi, V. Galdi, A. Alù, N. Engheta, Metastructures for signal manipulation, in: 2013 USNC-URSI Radio Science Meeting (Joint with AP-S Symposium), 2013, pp. 231-231.
[17] W. Cai, V. Shalaev, Introduction, in: W. Cai, V. Shalaev (Eds.) Optical Metamaterials: Fundamentals and Applications, Springer New York, New York, NY, 2010, pp. 1-10.
[18] B. Li, K.T. Tan, Asymmetric wave transmission in a diatomic acoustic/elastic metamaterial, J. Appl. Phys., 120 (2016) 075103.
[19] B. Li, Y. Liu, K.-T. Tan, A novel meta-lattice sandwich structure for dynamic load mitigation, J. Sandw. Struct. Mater., (2017) 1099636217727144.
[20] J.-S. Hwang, T.-G. Choi, D. Lee, M.-Y. Lyu, D.G. Lee, D.-Y. Yang, Dynamic and static characteristics of polypropylene pyramidal kagome structures, Compos. Struct., 131 (2015) 17-24.
[21] Y. Shen, W. Cantwell, R. Mines, Y. Li, Low-velocity impact performance of lattice structure core based sandwich panels, J. Compos. Mater., 48 (2013) 3153-3167.
[22] H. Jin, H. Hao, Y. Hao, W. Chen, Predicting the response of locally resonant concrete structure under blast load, Constr. Build. Mater., 252 (2020) 118920.

[23] C. Xu, W. Chen, H. Hao, The influence of design parameters of engineered aggregate in metaconcrete on bandgap region, J. Mech. Phys. Solids., 139 (2020) 103929.
[24] F. Farzbod, M. Leamy, Analysis of Bloch's Method and the Propagation Technique in Periodic Structures, J. Vib. Acoust., 133 (2011) 031010.
[25] Y. Liu, X. Shen, X. Su, C.T. Sun, Elastic Metamaterials With Low-Frequency Passbands Based on Lattice System With On-Site Potential, J. Vib. Acoust., 138 (2016) 021011-021011-021010.
[26] P.A. Shirbhate, M.D. Goel, A Critical Review of Blast Wave Parameters and Approaches for Blast Load Mitigation, Archives of Computational Methods in Engineering, (2020).
[27] P. Tran, S. Linforth, T.D. Ngo, R. Lumantarna, T.Q. Nguyen, Design analysis of hybrid composite anti-ram bollard subjected to impulsive loadings, Compos. Struct., 189 (2018) 598-613.
[28] L.-C. Alil, L.-C. Matache, S. Sandu, Numerical Simulation of a Ballistic Impact on Tensylon® UHMWPE Laminates Using the Plastic Kinematic Model in LS-Dyna®, Journal of Military Technology, 1 (2018) 43-50.
[29] F. Qin, A. Tong, C. Na, Strain rate effect and Johnson-Cook models of lead-free solder alloys, 2008.
[30] J.J.L.S.T.C. Hallquist, LS-Dyna Theory manual, March 2006, (2012).
[31] H.H. Huang, C.T. Sun, Wave attenuation mechanism in an acoustic metamaterial with negative effective mass density, New J. Phys., 11 (2009) 013003.
[32] R. Alberdi, J. Przywara, K. Khandelwal, Performance evaluation of sandwich panel systems for blast mitigation, Eng. Struct., 56 (2013) 2119-2130.
[33] C. Qi, S. Yang, L.-J. Yang, Z.-Y. Wei, Z.-H. Lu, Blast resistance and multi-objective optimization of aluminum foam-cored sandwich panels, Compos. Struct., 105 (2013) 45-57.
[34] F.G. Friedlander, G.I. Taylor, The diffraction of sound pulses I. Diffraction by a semi-infinite plane, Proceedings of the Royal Society of London. Series A. Mathematical and Physical Sciences, 186 (1946) 322-344.
[35] H.N.G. Wadley, K.P. Dharmasena, M.Y. He, R.M. McMeeking, A.G. Evans, T. Bui-Thanh, R. Radovitzky, An active concept for limiting injuries caused by air blasts, Int J Impact Eng, 37 (2010) 317-323.

List of Figures

Fig. 20. Outline model utilized for the calculation of (a) k_2 and k_4, and (b) k_1 and k_3.

List of Tables

Appendix

With an attempt to estimate the accurate values of the spring stiffness k_i (i=1,2,3,4), the commercial software COMSOL MULTIPHYSICS was leveraged to conduct the numerical simulation. A constant force F which is depicted in Fig. 20 (a) is applied to the model to calculate the value of shear spring stiffness k_2 of the internal core and while two constant force F was put in two directions of the model to estimate the values of k_1 shown in Fig. 20(b). Similarly, the calculation of value k_4 and k_3 is carried out with the same procedure but different dimensions. As seen in Fig. 20 (a) and 20 (b), the average displacements monitored at the surfaces are denoted as u_i (i=1,2,3,4) and captured by commercial software. The boundary condition for all edges of the outer shell is clamped. The relation between stiffness and displacement of the unit model which is shown in will be achieved as following [19]:

$$k_1\left(u_1+u_2\right)+k_2u_1=F \tag{30}$$

$$k_2u_3=F$$

$$k_3\left(u_4+u_5\right)+k_4u_4=F$$

$$k_4u_6=F$$

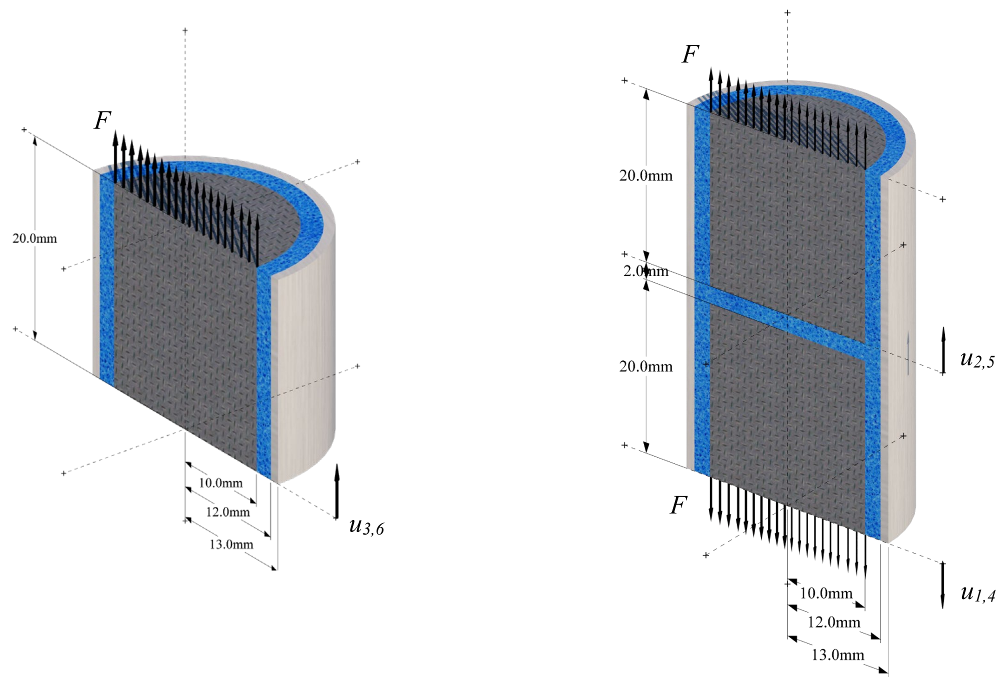

(a) (b)

Fig. 20. Outline model utilized for the calculation of (a) k_2 and k_4, and (b) k_1 and k_3.

704